The International Journal of Advanced Manufacturing Technology (2023) 130:1855–1869
https://doi.org/10.1007/s00170-023-12707-0

ORIGINAL ARTICLE

Numerical and analytical estimation of rolling force and torque in hot strip rolling

Aldo Attanasio[1] · Antonio Del Prete[2] · Teresa Primo[2]

Received: 24 May 2023 / Accepted: 21 November 2023 / Published online: 14 December 2023

Abstract

In this paper, both numerical and analytical method were developed for computing, in strip or plate rolling, the distribution of roll pressure, rolling force, and rolling torque (from which also rolling power can be estimated), assuming an homogeneous deformation of the rolled material. Unlike other similar models present in the literature, which solve the resulting rolling differential equation for the roll pressure, the model presented in this work solves the problem for the horizontal force. In this way, it is possible to avoid the calculation of the derivative of material flow stress curve, which is not always analytically easy and possible (i.e., point material flow stress data). The proposed numerical model is based on the friction law proposed by Chen and Kobayashi while the analytical one is based on the simple shear friction model and brings to useful analytical formulas for a quick calculation of rolling torque and force. Moreover, a relationship between the shear friction factor and Coulomb friction coefficient in rolling was found. The developed models show good agreement with experimental measures, in terms of rolling force and torque, found in literature.

Keywords Hot strip rolling · Numerical modeling · Analytical modeling · Rolling force · Torque

Nomenclature

a	Kobayashi friction constant (mm/s)
C(T)	Material flow stress law parameter (MPa)
F	Axial force along x (N/mm)
F_1	Back tension force (N/mm)
F_2	Front tension force (N/mm)
h	Height of the rolled material al the considered section (mm)
h_n	Height of the rolled material at neutral point (mm)
h_1	Original height of the rolled material (mm)
h_2	Final height of the rolled material (mm)
k	Yield stress in plane strain (MPa)
m	Shear friction factor
m(T)	Material flow stress law strain rate exponent
N	Rolls angular velocity (RPM)
P	Vertical roll Force (N/mm)
Q	Volumetric rate (mm^2/s)
R	Rolls radius (mm)
s	Roll pressure (N/mm^2)
t	Friction stress (N/mm_2)
T	Rolling torque on a roll (N•mm/mm)
V	Strip material velocity (mm/s)
V_x	Component of strip material velocity V along x axis (mm/s)
V_{rel}	Relative velocity between VR and strip velocity V
VR	Rolls peripheral velocity (mm/s)
θ	Angular coordinate from plane of roll axes (rad)
θ_n	Value of θ at the neutral point (rad)
α	Value of θ at entry section (rad)

✉ Teresa Primo
teresa.primo@unisalento.it

Aldo Attanasio
aldo.attanasio@unibs.it

Antonio Del Prete
antonio.delprete@unisalento.it

[1] University of Brescia, via Branze 38, 25123 Brescia, Italy

[2] Department of Engineering for Innovation, University of del Salento, Viale per Monteroni, 73100 Lecce (LE), Italy

1 Introduction

Rolling is the most widely used mechanical work technique. About three quarters of steel output is treated in rolling mills, and only a quarter is consumed for forging, extruding, and founding [1].

Recent review papers on rolling process [2, 3] continues to point out that there are new demands on modeling the

rolling process that could bring prompt answers for industrial need. Experimental methods require expensive equipment and a large number of reproductive tests [4].

In the past, especially in the beginning of twentieth century when computer did not exist, many attempts were made in order to develop simple analytical models of rolling, able to estimate macroscopic process parameters like roll force and torque. They are important parameters in hot strip rolling, as they affect the quality of the final product and the efficiency of the rolling process. One fundamental requirement for fully automatic operation of hot strip mills is the calculation of rolling force in each rolling stand by mathematical models. The accuracy and precision levels achieved by those models depend also on specific features of each hot strip mill line.

During the last three decades, finite elements methods have known great advances in their application in the rolling process analyses, [5–8]. These methods are based on powerful software permitting to carry out fine details and analyses but they are still leading to a complex solution process and massive computational time.

Analytical methods [9–11] are most suitable and commonly used in industry. There are several models that have been developed where mechanical and physical parameters of the rolling process can be predicted rapidly in some confidence. As far as thin strips are concerned, the slab method is the most appropriate [3] and knows improvement according to the industrial needs.

The slab method [12, 13, 14] is probably the most commonly used continuum mechanics-based approach to create fast rolling models [15]. The popularity of slab models can likely be attributed to the low complexity and the arbitrary extensibility [16, 17, 18].

Accurate information on rolling loads are useful when designing a rolling pass schedule. Many studies are focused on hot and cold plain rolling (i.e., plate or strip rolling), and one of the most used technique to solve the problem is the use of the slab method coupled with some simplifying physical assumption (i.e., plain strain deformation, material rigid plastic behavior, etc.).

This technique is surely less comprehensive than latest developed such as the FEM but, at the same time, it is less expensive from a computational point of view and allows to explain many issues of the roll bite mechanics. Furthermore, thanks to their simplicity, many rolling models used in the R&D centers of metallurgical companies are still based on this kind of approach [19].

Several models have been then developed in the past in order to better understand plain rolling process. Probably the first one was developed by Von Karman [20] that described the roll pressure distribution along the arc of contact between roll and workpiece by means of a differential equation, starting from the assumption of homogenous deformation. This assumption states that plane sections remain plane during the deformation under the roll bite. Bland and Ford [21] obtained an analytical solution for the estimation of the neutral angle, with the hypotheses of homogenous deformation, small angle simplification and slipping friction described by Coulomb's law. However once the neutral point is calculated, roll force and torque cannot be analytically obtained and, as a consequence, the numerical calculation is needed. Bland and Ford [23] also proposed a model taking into account elastic deformation of contact arcs in entry and exit zones of roll bite. Orowan's theory [24] considered the case of a not homogeneous deformation introducing an adjusting factor. Moreover in his model, Orowan considered both slipping and sticking friction cases. In order to perform calculation of his comprehensive theory, Orowan had to use a complicate graphical-numerical method.

With the aim to avoid uncomfortable computation methods necessary to solve Orowan's model, Sims [25, 26] solved analytically Orowan's equation for the sticking friction case introducing small angle simplification and considering a material with a constant yield stress. Sims derived algebraic formulae for neutral angle, roll pressure distribution, roll force, and roll torque. Sims's model is largely used in industrial rolling process control. Alexander [27] proposed a model based on homogeneous deformation assumption and with a mixed friction law. In this model, once friction force reached the material shear yield stress, the model automatically switch from slipping friction to sticking friction. Alexander included the strain-hardening effect of the rolled material; thus, in the resulting differential equation appears the derivative of the material flow stress curve. Alexander used the forth order Runge-Kutta solver scheme in order to reach numerical solution of roll pressure and then to obtain roll force and torque. Pietrzyk and Lenard [28] developed a refinement of the models of Alexander and Ford. Gunasekera [29] proposed similar numerical model with a constitutive equation for the material flow stress which included the effect of strain, strain rate, and temperature. Moreover, in [29], a friction model suitably modified to match the pressure calculated distribution with experimental data was implemented. Rusia [30] improved Alexander's model introducing the model of friction proposed by Chen and Kobayashi [31]. This friction model utilizes a suitable mathematical form in order to consider null friction forces in the neutral angle zone, where the relative velocity between the rolled material and rolls are very small or equal to zero. Venter and Abd-Rabbo [32, 33] developed a computerized model for both hot and cold rolling taking into account inhomogeneity of deformation. Freshwater [34] simplified the equations proposed by Alexander [27] and Venter and Abd-Rabbo [32, 33] by removing the derivative of material flow stress curve. None of previous model was taking into account shear stresses. Lalli [35] developed an

analytical solution for the calculation of roll force and torque taking into account shear stresses role with a homogeneous deformation model. Hu [36, 43] developed a model for the calculation of vibration on the mill structure due to rolling process, by means of both homogenous and inhomogeneous deformation assumptions. Chun and Lenard [44] compared experimental measurement of rolling torque and load with a numerical slab method based on Coulomb friction law, demonstrating that when the ratio between roll and rolled thickness is sufficiently high, homogenous hypothesis is reasonable and can bring to good agreement. A wide review of the existing method of rolling analysis can be found in [19] and [56].

Yang et al., [37] investigated the influence of the vertical movement velocity of the rolls on the rolling process. A dynamic model for the rolling process when the roll gap is decreased during the dynamic hot rolling process was proposed. The work in [38] shows an alternative methodology for direct calculation of rolling force by using the empirical equation proposed by Schultz [39]. A new solution Karman's equation with the Mises plasticity condition was proposed in [40] for determining contact stresses in the slip zones for hot strip rolling. It was demonstrated that, even when dealing with elevated frictional coefficients, the extent of slip zones comprises a noteworthy portion of the deformation region's length. Using the solutions acquired, enhancements were made to the methods for graphing normal contact stress curves, ascertaining slip zone lengths, pinpointing the neutral position of the cross-section, and refining the calculation of rolling force.

Rolling force is one of the significant parameters in rolling process planning and equipment design, which is important for the normal operation of equipment. Accurate calculation of rolling force is the key to produce high quality strip. Li et al. proposed a new analytical model for the prediction of rolling force based on the tangent velocity field and linear MY (mean yield) criterion in hot strip rolling [41].

Li et al. proposed a novel 3D multi-stand coupled thermomechanical finite element (FE) model for the THR tandem hot rolling developed employing a segmentation modeling strategy and data transfer technologies [42]. From the study of the literature, it was found that the different models are characterized by a different level of complexity and simplifications, all correctly validated.

In the present paper, a numerical homogeneous model based on the friction law proposed by Chen and Kobayashi [31] was developed. Differently to other similar models [27, 30], which solve the resulting differential equation for the roll pressure, the model presented in this work solves the problems for the horizontal force in the strip. In this way, it is possible to avoid the calculation of the derivative of material flow stress curve, which is not always analytically easy and possible (i.e., point material flow stress data). In addition, an analytical closed solution of the problem, based on simple shear friction model, is provided. Useful analytical formulas for a quickly calculation of rolling torque and load were developed. Finally, both numerical and analytical models, in terms of roll force and torque calculation, were validated through the comparison with literature experimental data [44]. The aim was to propose and to provide an enabling methodology. Therefore, anyone, once they know the methodology proposed in the paper, will also be able to apply and validate it to compare other cases, experimental data sets of their own or from several literature sources.

2 Mathematical model

In the present work, the following assumptions have been assumed in the proposed mathematical model formulation:

1. The strip material is assumed to have a rigid-plastic behavior with strain-hardening effects with incompressibility condition. As a consequence:

$$\dot{\varepsilon}_x + \dot{\varepsilon}_y + \dot{\varepsilon}_z = \varepsilon_x + \varepsilon_y + \varepsilon_z = 0 \tag{1}$$

2. Deformation occurs under plane strain conditions; therefore, no change in strip width is considered [45–52]. Then:

$$\dot{\varepsilon}_z = \varepsilon_z = 0 \tag{2}$$

3. Following the slab method, strain and stresses do not vary in the thickness direction; they are independent of y direction.
4. Von Mises yield criterion has been applied, neglecting shear stresses due to shear deformation. As a consequence, only normal stresses have been considered in the analysis.
5. Friction force has been modeled by Chen and Kobayashi's arc tangent function [31].
6. The rolls are considered as rigid bodies [58, 59].

With reference to Fig. 1, the balance of the forces applied to all the sides of the slab in the rolling direction (x axis) leads to the basic first order differential Eq. (3). It is important to highlight that assumption 3 is reasonable until the ratio thickness over work-roll radius is maintained low. On the basis of what is reported in the literature [53–55], in the case of plates or sheets, in particular for ratios equal to approximately 5, justify the simplification. In the specific case considered in the present work, it is in the order of approximately equal to 8.3; therefore, the simplifying hypothesis of deformation plane state is more than reasonable.

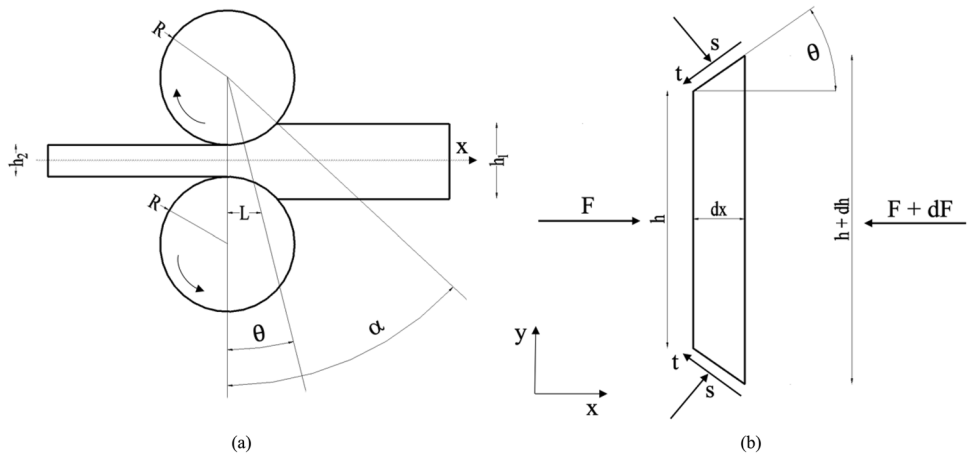

Fig. 1 **a** Geometry of the roll bite; **b** forces acting on a slab element in the roll bite

If this ratio increases, the heterogeneity of the deformation across thickness direction increases and cannot be neglected [57].

$$\frac{\partial F}{\partial \theta} = -2R\cos\theta(s\tan\theta \pm t) \tag{3}$$

Where:

- F is the axial force along x (N/mm)
- R is the roll radius (mm)
- θ is the angle varying from α (entry section) to 0 (exit section) (rad)
- s is the roll pressure (N/mm^2)
- t is the friction stress (N/mm^2)
- $+$ sign is for the exit section
- $-$ sing is for the entry section

It is possible to note that all quantities are normalized along the strip width. Regarding to the $\pm$ symbol (or vice versa), in this work, the upper sign refers to the exit section (from $\theta = 0$ to $\theta = \theta_n$ where θ_n is the angle of the neutral point) while the lower sign refers to entry section (from $\theta = \theta_n$ to $\theta = \alpha$).

Neglecting shear stress contribution, the yield criterion of Von Mises for the plain strain condition leads to [21, 22]:

$$\sigma_x - \sigma_y = k = \frac{2}{\sqrt{3}} \cdot \sigma_{eq} \tag{4}$$

where σ_{eq} is the material flow stress. The equilibrium of forces along the vertical axis y leads to:

$$\sigma_y = -(s \mp t\tan\theta) \tag{5}$$

considering a mean stress along x axis on a strip section of thickness h:

$$\sigma_x = \frac{F}{h} \tag{6}$$

with:

$$h = h_2 + 2R(1 - \cos\theta) \tag{7}$$

friction force has been modelled with the shear model modified by Kobayashi and Chen [11]:

$$t = m\frac{\sigma_{eq}}{\sqrt{3}}\left\{\left(\frac{2}{\pi}\right)\tan^{-1}\left(\frac{V_{rel}}{a}\right)\right\} = m\frac{k}{2}\left\{\left(\frac{2}{\pi}\right)\tan^{-1}\left(\frac{V_{rel}}{a}\right)\right\} = m\frac{k}{2}G \tag{8}$$

with:

$$G = \left\{\left(\frac{2}{\pi}\right)\tan^{-1}\left(\frac{V_{rel}}{a}\right)\right\} \tag{9}$$

- V_{rel} is the relative velocity between peripheral speed of the rolls V_R and the strip velocity V
- a, the Kobayashi friction constant, is a constant several orders of magnitude less than V_R

combining equations from 3 to 9 leads to:

$$\left\{\frac{\partial F}{\partial \theta} = -2R\cos\theta\left[-\frac{F}{h(\theta)} + \frac{k}{2}\left(2\tan\theta \pm m|G|(\tan\theta)^2 \pm m|G|\right)\right]\right. \tag{10}$$

$$F(\alpha) = F_1 \tag{11}$$

$$F(0) = F_2 \tag{12}$$

This differential equation, in which the unknown is the function F, describes the strip rolling process. Equations (11) and (12) explain boundary conditions, which are related to the presence or not of back and front tension here called with F_1 and F_2.

In order to solve Eq. (10) it is necessary to know k which depends by the material flow stress (Eq. 4). Flow stress can generally depend by strain, strain rate and temperature.

$$\sigma_{eq} = f\left(\varepsilon_{eq}, \dot{\varepsilon}_{eq}, T\right) \tag{13}$$

Strain in each strip section can be calculated as follows:

$$\varepsilon_y = \ln\frac{h}{h_1} \tag{14}$$

from incompressibility condition (Eq. 1) and plane strain condition (Eq. 2) it can be found that:

$$\varepsilon_x = -\varepsilon_y \tag{15}$$

finally, the equivalent strain necessary for flow stress calculation can be calculated from:

$$\varepsilon_{eq} = \sqrt{{}^2\!/_3\,(\varepsilon_x^2 + \varepsilon_y^2)} \tag{16}$$

regarding strain rate it can be observed that in a dt time strip thickness, in a generic section, is reduced by dh, then [24]:

$$\dot{\varepsilon}_y == \frac{1}{h}\frac{dh}{dt} = \frac{1}{h}\frac{dh}{dx}\frac{dx}{dt} = \frac{1}{h}\frac{dh}{d\theta}\frac{d\theta}{dx}\frac{dx}{dt} = \frac{1}{h}\frac{dh}{d\theta}\frac{d\theta}{dx}V_x \tag{17}$$

V_x can be calculated in each strip section from:

$$V_x = \frac{Q}{h} \tag{18}$$

where Q is the volumetric rate measured in [mm^2/s]. Substitution of Eq. 18 in Eq. 17 leads to [5]:

$$\dot{\varepsilon}_y = 2Q\frac{\tan\theta}{h^2} \tag{19}$$

in a similar way to what has been done to find the equivalent strain, equivalent strain rate can be calculated as:

$$\dot{\varepsilon}_{eq} = \sqrt{{}^2\!/_3\,(\dot{\varepsilon}_x^2 + \dot{\varepsilon}_y^2)} \tag{20}$$

from Eq. 17, it is possible calculate the mean strain as [7]:

$$\overline{\dot{\varepsilon}_y} = \frac{1}{\alpha}\int_0^{\alpha}\dot{\varepsilon}_y d\theta = \frac{1}{\alpha}\frac{2\pi N}{60}\left[\ln\left(\frac{h_1}{h_2}\right)\right] \tag{21}$$

where N is the revolutions per minute of the rolls. It is important to note that the exact value of Q depends on the position of the neutral point that is defined as the point in which strip velocity is equals to rolls peripheral velocity. Before this point, friction forces acting on strip surfaces are directed towards the exit section; after this point, friction forces act towards the entry section. Unfortunately, the exact location of the neutral point is not known a priori. As a consequence, strain rate distribution (given by Eq. 19) cannot be known, and then also flow stress distribution within the strip cannot be calculated (see Eq. 13). The ways to overcome this problem will be explained for numerical and analytical solving of Eq. 10 in Sections 3 and 4, respectively.

3 Numerical solution

Equation 10 is generally not solvable analytically unless mathematical simplifications. In this section, none of these simplifications were introduced; consequently, the solution was obtained numerically. In order to obtain a solution, a first discretization of the domain of integration [0; α] have to be done. In this paper, classical Runge–Kutta method (RK4) was employed to solve Eq. 10. This is a fourth-order explicit method that requests, for each point of the discretized domain, four new evaluations of the unknown function F. More details about this method can be found in [57]. In order to overcome the difficulty given by the indetermination of the neutral point and then of the volume rate Q, a first hypothesis on the neutral point location is done in order to have a first Q estimation, which allows to solve Eq. 10.

To solve Eq. (10), it is necessary to know the flow stress of the material which depends by the strain, strain rate, and temperature. To evaluate the strain rate, it is necessary to know the volumetric flow rate which can be determined if the neutral angle is known. The latter is obtained by solving Eq. 10. The problem is therefore non-linear and was solved by iteration, that is:

1. An initial neutral angle was assumed;
2. The volumetric flow rate was calculated;
3. The strain and strain rate were calculated, so it was possible to calculate the flow stress in each section of the strip;
4. Eq. 10 has been solved;
5. Another neutral angle value was found;
6. Steps 2) to 5) were repeated until the values relating to the neutral angle converged. A convergence rule has been imposed in the code which must be less than/equal to 0.5%, i.e., the neutral angle value is considered acceptable when it differs by a maximum of 0.5% from the old value.

Once numerical solution of F is known, the roll pressure s can be found from Eq. 5 using Eqs. 4, 6, and 8 as:

$$\begin{cases} s_1 = -\frac{F_1}{h} + k - m\frac{k}{2}|G|\tan\theta \\ s_2 = -\frac{F_2}{h} + k + m\frac{k}{2}|G|\tan\theta \end{cases} \tag{22}$$

where F_1 and F_2 are solution of Eq. 10 for the entry and exit sections, respectively, and s_1 and s_2 are the related values of roll pressure. Values of s_1 are valid for $\theta \in [\theta_n; \alpha]$ while values of s_2 are valid for $\theta \in [0; \theta_n]$. Figure 2, instead, shows an example of the final roll pressure distribution.

Figure 3 shows an example the final roll pressure distribution.

The intersection of s_1 and s_2 plots returns the angle θ_n from which corresponding strip thickness h_n can be calculated putting $\theta=\theta_n$ in Eq. 7. Then, volume rate can be recalculated as:

$$Q = h_n V_R \cos\theta_n \tag{23}$$

The new value of Q allows to recalculate F from Eq. 10, and then the solution procedure can be iterated until convergence of Q is reached. In this paper, the first value of Q is calculated by means of Eq. 23 supposing starting value of neutral point given by:

$$\theta_{n\_start} = 0.75\alpha \tag{24}$$

Once convergence is reached, remembering that friction forces change versus at the neutral point, rolling torque T and load P per unit of width on the roll can be calculated from:

$$T = R^2\left[-\int_0^{\theta_n} t d\theta + \int_{\theta_n}^{\alpha} t d\theta\right] \tag{25}$$

$$P = R\left[\int_0^{\theta_n} s_2\cos\theta d\theta + \int_{\theta_n}^{\alpha} s_1\cos\theta d\theta - \int_0^{\theta_n} t\sin\theta d\theta + \int_{\theta_n}^{\alpha} t\sin\theta d\theta\right] \tag{26}$$

where t is expressed by Eq. 8. In this work, Eqs. 25 and 26 were solved by trapezoidal integration rule. It is important to consider that Eq. 26 takes into account also the contribution of friction forces that generally in literature are neglected. From the distribution of friction forces, it is possible to inversely calculate a corresponding value of the Coulomb friction factor μ. In fact:

$$t = \mu \cdot s = m \cdot \frac{k}{2} \tag{27}$$

then:

$$\mu = \frac{m \cdot k}{2 \cdot s} \tag{28}$$

Since k and s generally change in the roll bite, Eq. 28 returns different values in terms of μ. Typically in literature [27], mathematical modeling of hot rolling with shear friction model was used to consider that when values of Coulomb

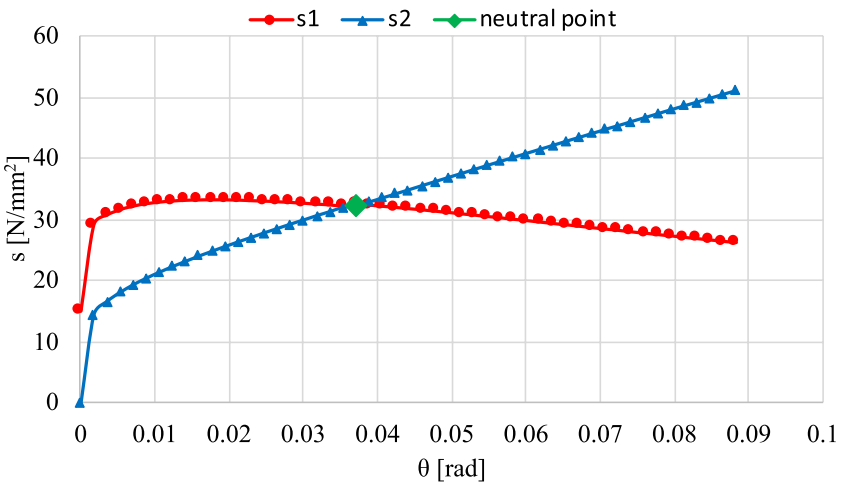

Fig. 2 Predicted distribution pressure calculated from the entry section (s1) and from the exit section (s2); intersection of the two curves identifies the neutral point

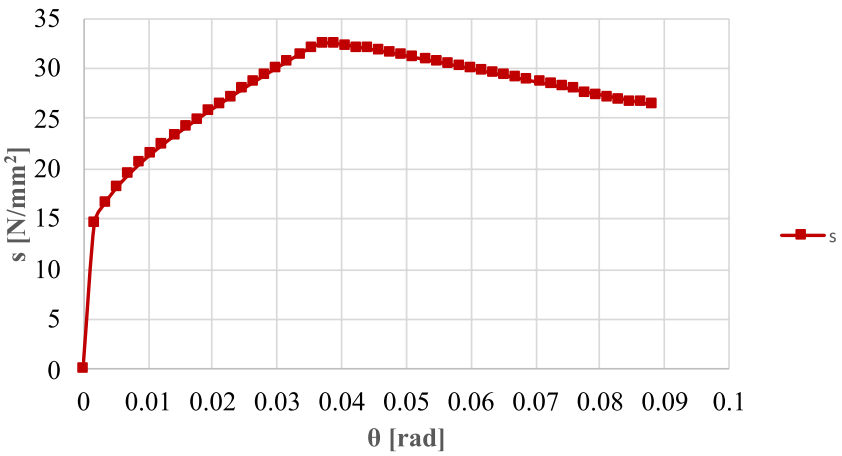

Fig. 3 Resulting effective distribution of the calculated roll pressure with the numerical model

coefficient μ are too high, friction forces could overcome material flow stress, which is physically not possible. Based on these considerations, only the maximum value of μ obtained by means of Eq. 28 has been considered. The maximum value of μ occurs when s is minimum. Depending on material flow stress law and boundary conditions in terms of back and front forces (F_1 and F_2, respectively), s can be minimum at the entry or exit section and reach a maximum value in correspondence of the neutral point (see Fig. 3). Then:

$$\mu = max\begin{cases} \frac{m\cdot k(\alpha)}{k(\alpha)\cdot[2-m\cdot\tan\alpha]-2\frac{F_1}{h_1}} \\ \frac{1}{2}\frac{m\cdot k(0)}{k(0)-\frac{F_2}{h_2}} \end{cases} \tag{29}$$

in the particular case in which $F_1 = F_2 = 0$:

$$\mu = max\begin{cases} \frac{m\cdot k(\alpha)}{k(\alpha)\cdot[2-m\cdot\tan\alpha]} \\ \frac{1}{2}\frac{m\cdot k(0)}{k(0)} \end{cases} = \frac{m}{[2-m\cdot\tan\alpha]} \tag{30}$$

4 Analytical solution

In order to find an analytical resolution of Eq. 10, according to [26], the following mathematical simplifications were introduced:

$$\begin{cases} \sin\theta \approx \tan\theta \approx \theta \\ \cos\theta \approx 1 - \frac{\theta^2}{2} \end{cases} \tag{31}$$

note that these are the same simplification made in [26]. This leads to an approximate form of Eq. 7 as:

$$h = h_2 + R\theta^2 \tag{32}$$

as a consequence, Eq. 3 becomes:

$$\frac{\partial F}{\partial \theta} = \frac{\partial(\sigma_x h)}{\partial \theta} = -2R\left[\theta s \pm \left(1 - \frac{\theta^2}{2}\right)t\right] \tag{33}$$

friction model given by Eq. 8 was reduced neglecting function G. Then friction model can be expressed by:

$$t = m\frac{\sigma_{eq}}{\sqrt{3}} = m\frac{k}{2} \tag{34}$$

Equation 22 becomes:

$$s = -\sigma_x + k \pm m\frac{k}{2}\theta \tag{35}$$

from which:

$$\sigma_x = -s + k \pm m\frac{k}{2}\theta \tag{36}$$

replacing Eqs. 34 and 36 in Eq. 33 and solving for s yields:

$$\frac{\partial s}{\partial \theta} = \frac{\partial k}{\partial \theta}\left[1 \pm \frac{m\theta}{2}\right] \pm \left[\frac{mk}{2}\right] \pm \left[\frac{Rmk}{h}\right] \pm \frac{R\theta^2}{2h}mk + \frac{2R\theta k}{h} \tag{37}$$

in order to integrate directly Eq. 33, k is replaced by a constant mean value calculated overall for the entire roll bite:

$$\bar{k} = \frac{1}{\alpha}\int_0^{\alpha} k d\theta = constant \tag{38}$$

this implies that:

$$\frac{\partial \bar{k}}{\partial \theta} = 0 \tag{39}$$

substitution of Eq. 34 and 35 in Eq. 33 leads to:

$$\begin{cases} \frac{\partial s}{\partial \theta} = \left[\frac{m\bar{k}}{2}\right] \pm \left[\frac{Rm\bar{k}}{h}\right] \pm \frac{R\theta^2}{2h}m\bar{k} + \frac{2R\theta\bar{k}}{h} \end{cases} \tag{40}$$

$$\begin{cases} s(\theta = \alpha) = s_{1o} = \bar{k} - \sigma_{1o} - m\frac{\bar{k}}{2}\alpha = \bar{k} - \frac{F_1}{h_1} - m\frac{\bar{k}}{2}\alpha \end{cases} \tag{41}$$

$$\begin{cases} s(\theta = 0) = s_{2o} = s_{1o} = \bar{k} - \sigma_{2o} = \bar{k} - \frac{F_2}{h_2} \end{cases} \tag{42}$$

where Eqs. 41 and 42 are the related boundary conditions obtained from Eq. 35. As it can be seen, σ_{2o} and σ_{1o} are the stresses due to front and back tension, respectively, in exit and entry sections.

Integration of Eq. 40 results in:

$$\begin{cases} s_1 = [s_{1o}] + \bar{k}\ln\left(\frac{h}{h_1}\right) + m\bar{k}\alpha + m\bar{k}\left[\sqrt{R/h_2}\,Z(\alpha)\right] - m\frac{\bar{k}}{2}\frac{Z(\alpha)}{\sqrt{R/h_2}} - m\bar{k}\theta - m\bar{k}\left[\sqrt{R/h_2}\,Z(\theta)\right] + m\frac{\bar{k}}{2}\frac{Z(\theta)}{\sqrt{R/h_2}} \\ s_2 = [s_{2o}] + \bar{k}\ln\left(\frac{h}{h_2}\right) + m\bar{k}\theta + m\bar{k}\left[\sqrt{R/h_2}\,Z(\theta)\right] - m\frac{\bar{k}}{2}\frac{Z(\theta)}{\sqrt{R/h_2}} \end{cases} \tag{43}$$

where:

$$Z(\theta) = \tan^{-1}\left(\theta\sqrt{{}^{R}/_{h_2}}\right) \tag{44}$$

The angle related to the neutral point can be found equating s_1 with s_2 and solving for θ:

$$\theta_n = \frac{1}{2m\bar{k}}\left\{\left[\sigma_{2o} - \sigma_{1o}\right] - \bar{k}\ln\left(\frac{h_1}{h_2}\right) + m\bar{k}\left[\frac{\alpha}{2} + \sqrt{{}^{R}/_{h_2}}Z(\alpha) - \frac{Z(\alpha)}{2\sqrt{{}^{R}/_{h_2}}}\right] - mk\left[2\sqrt{{}^{R}/_{h_2}}Z(\theta_n) - \frac{Z(\theta_n)}{\sqrt{{}^{R}/_{h_2}}}\right]\right\} \tag{45}$$

Equation 45 is a nonlinear equation that can be solved graphically or through specific numeric methods (i.e., Newton–Raphson or fixed-point iteration). However, it is possible to find an analytical closed form by noting that usually θ_n assumes values near zero. Then the following approximation can be introduced in Eq. 45:

$$Z(\theta_n) = \tan^{-1}\left(\theta_n\sqrt{{}^{R}/_{h_2}}\right) \approx \theta_n\sqrt{{}^{R}/_{h_2}} \tag{46}$$

It is important to note that this approximation was adopted only for $Z(\theta_n)$ and not for $Z(\alpha)$, because in this last case is not necessary. Replacing Eq. 46 in Eq. 45 and solving for θ_n yields:

$$\theta_n = \frac{1}{2m\bar{k}}\frac{\left\{\left[\sigma_{2o} - \sigma_{1o}\right] - \bar{k}\ln\left(\frac{h_1}{h_2}\right) + m\bar{k}\left[\frac{\alpha}{2} + \sqrt{{}^{R}/_{h_2}}Z(\alpha) - \frac{Z(\alpha)}{2\sqrt{{}^{R}/_{h_2}}}\right]\right\}}{\left[{}^{R}/_{h_2} + {}^{1}/_{2}\right]} \tag{47}$$

Once θ_n is known, it is possible to proceed with the calculation of rolling torque T and load P per unit of width. From integration of Eq. 25, introducing simplifications given by Eq. 31, Eq. 34 and results of Eq. 43:

$$T = R^2 m\frac{\bar{k}}{2}\left[\alpha - 2\theta_n\right] \tag{48}$$

If rolling torque and material mean flow stress are experimentally known, founding neutral point through Eq. 47 and then solving Eq. 48 for the shear factor m can be interesting in order to have quickly an estimation of rolling friction conditions.

Regarding rolling load the following approximate method of calculation was employed [24–26]:

$$P = R\left[\int_0^{\theta_n} s_2\cos\theta d\theta + \int_{\theta_n}^{\alpha} s_1\cos\theta d\theta - \int_0^{\theta_n} t\sin\theta d\theta + \int_{\theta_n}^{\alpha} t\sin\theta d\theta\right] \approx R\left[\int_0^{\theta_n} s_2 d\theta + \int_{\theta_n}^{\alpha} s_1 d\theta\right] \tag{49}$$

Replacing s_1 and s_2 from Eq. 43:

$$P = R\left\{\left[\theta_n\left(s_{2o} - s_{1o}\right) + s_{1o}\alpha\right] + \bar{k}\theta_n\ln\left(\frac{h_1}{h_2}\right) - m\bar{k}B(\alpha) + 2m\bar{k}B\left(\theta_n\right) + \bar{k}\left[-2\alpha + \frac{2Z(\alpha)}{\sqrt{{}^{R}/_{h_2}}}\right] + m\bar{k}b(\alpha)\left[\alpha - \theta_n\right]\right\} \tag{50}$$

where:

$$b(\theta) = \theta + \sqrt{{}^{R}/_{h_2}}\,Z(\theta) - \frac{Z(\theta)}{2\sqrt{{}^{R}/_{h_2}}} \tag{51}$$

$$B(\theta) = \frac{\theta^2}{2} + Z(\theta)\left(\sqrt{{}^{R}/_{h_2}} - \frac{1}{2\sqrt{{}^{R}/_{h_2}}}\right)\theta + \left(\frac{1}{4\,{}^{R}/_{h_2}} - \frac{1}{2}\right)\ln\left({}^{R}/_{h_2}\,\theta^2 + 1\right) \tag{52}$$

Unlike Eq. 26, Eq. 50 was obtained neglecting friction force contribution but slightly overestimating the roll pressure contribution. This approach should result in a percentage error lower than 10% [24–26]. Similarly to the previous section, from the distribution of friction forces, it is possible to inversely calculate a corresponding value of the Coulomb friction coefficient μ. Considering Eqs. 28 and 29, it is possible to obtain:

$$\mu = max\begin{cases} \dfrac{m\cdot\bar{k}}{\bar{k}\cdot[2-m\cdot\alpha]-2\frac{F_1}{h_1}} \\ \dfrac{1}{2}\dfrac{m\cdot\bar{k}}{\bar{k}-\frac{F_2}{h_2}} \end{cases} \tag{53}$$

If $F_1 = F_2 = 0$, then:

$$\mu = max\begin{cases} \dfrac{m\cdot\bar{k}}{k\left[2-\ m\cdot\tan\ \alpha\right]} \\ \dfrac{1}{2}\dfrac{m\cdot\bar{k}}{\bar{k}} \end{cases} = \frac{m}{\left[2-m\cdot\ \alpha\right]} \tag{54}$$

5 Results and discussion

In order to validate both the numerical and analytical models proposed in the present work, the prediction of rolling torque and load were compared with rolling experimental results found in the paper of Chun and Lenard in [44]. Their study was focused on the effects of the rolling speeds, reduction and lubricant on the roll torque, load, forward slip, and surface on commercially pure aluminum strips. By matching the measured and calculated roll separating forces, roll torques, and the forward slip, the Coulomb coefficient of friction as a function of the process parameters is obtained, too.

5.1 Experimental setup and measurement

In [44], commercially pure aluminum strips (Al1100-H14) of 6.12–6.16 mm thickness, 50–52 mm width, and 310 mm length were rolled at 500 °C. A reduction of approximately 15% and 35% was performed on the strips. Each reduction was replicated with a roll speed of 20, 60, 100, and 160 rpm. Generally, increasing hot-rolling reduction is an effective approach to improve overall mechanical properties and microstructure evolution of the material. For this reason and taking into account that in the case of plates with ratios equal to approximately 5 [53–55] (equal to about 8.3 in the present work), the variation in the width of the strip was not considered in the paper [45–52]; therefore, the simplifying hypothesis of deformation plane state is more than reasonable.

All the tests were done with two different lubricants with different emulsion concentrations. Both lubricants were based on synthetic esters, especially designed for hot rolling operations, and are referred in this work as semi-synthetic A, designed for low friction applications and semi-synthetic B, designed for higher friction applications. Rolling experiments were performed on a mill equipped with rolls having 127 mm radius and 100 mm length. Rolling torque was measured by transducers positioned in the driven spindles, while rolling force was measured by two load cells located under the bearing blocks of the lower roll. More details can be found in the paper [44].

5.2 Material flow stress characterization

It is known that, the goodness of the results produced by a mathematical modeling of a metal forming process strongly depends on accurate material flow stress data. Chun and Lenard [44] conducted flow stress characterization on the aluminum used in their study at temperatures and strain rates of interest. They expressed the flow stress in the following constitutive equation:

$$\begin{cases} \sigma_{eq} = C(T)\dot{\varepsilon}_{eq}^{m(T)} \\ C(T) = 76.887 - 0.1212T \\ m(T) = 0.0004T - 0.0258 \end{cases} \tag{55}$$

Table 1 Comparison of predicted and measured parameters

Test	Lubricant	h_1	$r_{\%}$	RPM	μ [19]	m	Experimental		Numerical		Error %		Analytical		Error %	
							P [N/mm]	T [Nm/mm]	P [N/mm]	T [Nm/mm]			P [N/mm]	T [Nm/mm]		
1	A_1	6.15	16.1	20	0.2	0.35	326	3650	300	3747	−7.98%	2.66%	297	3556	−8.90%	−2.58%
2	A_1	6.13	15.82	60	0.15	0.15	325	3740	323	3848	−0.62%	2.89%	321	3605	−1.23%	−3.61%
3	A_1	6.13	15.73	100	0.1	0.11	320	3940	341	4026	6.56%	2.18%	340	3785	6.25%	−3.93%
4	A_1	6.12	15.78	160	0.09	0.09	333	4030	363	4068	9.01%	0.94%	364	4043	9.31%	0.32%
5	A_1	6.12	34.48	20	0.2	0.7	691	9990	628	10883	−9.12%	8.94%	616	10927	−10.85%	9.38%
6	A_1	6.13	34.75	60	0.13	0.35	646	9900	603	10328	−6.66%	4.32%	594	9973	−8.05%	0.74%
7	A_1	6.14	35.18	100	0.12	0.24	633	9870	601	10338	−5.06%	4.74%	593	9859	−6.32%	−0.11%
8	A_1	6.14	35.34	160	0.14	0.18	650	10300	612	10609	−5.85%	3.00%	605	10029	−6.92%	−2.63%
9	A_{10}	6.13	16.38	20	0.18	0.4	337	3840	310	3932	−8.01%	2.40%	307	3744	−8.90%	−2.50%
10	A_{10}	6.16	15.58	60	0.18	0.2	314	4200	330	3960	5.10%	−5.71%	328	3713	4.46%	−11.60%
11	A_{10}	6.15	15.28	100	0.08	0.18	368	4140	353	4169	−4.08%	0.70%	350	3907	−4.89%	−5.63%
12	A_{10}	6.16	16.07	160	0.09	0.09	341	4090	368	4125	7.92%	0.86%	368	4143	7.92%	1.30%
13	A_{10}	6.12	34.26	20	0.22	0.67	668	9940	613	10604	−8.23%	6.68%	602	10606	−9.88%	6.70%
14	A_{10}	6.12	35.24	60	0.18	0.34	639	9920	604	10387	−5.48%	4.71%	594	10015	−7.04%	0.96%
15	A_{10}	6.14	35.18	100	0.12	0.23	616	9810	595	10233	−3.41%	4.31%	587	9749	−4.71%	−0.62%
16	A_{10}	6.13	35.24	160	0.1	0.22	679	10700	639	10993	−5.89%	2.74%	631	10466	−7.07%	−2.19%
17	B_1	6.16	15.75	20	0.28	0.39	312	3570	302	3760	−3.21%	5.32%	299	3576	−4.17%	0.17%
18	B_1	6.16	15.58	60	0.18	0.18	335	3780	327	3894	−2.39%	3.02%	324	3656	−3.28%	−3.28%
19	B_1	6.16	15.42	100	0.09	0.14	359	3950	346	4079	−3.62%	3.27%	344	3821	−4.18%	−3.27%
20	B_1	6.15	15.35	160	0.07	0.09	345	4070	359	4005	4.06%	−1.60%	359	3947	4.06%	−3.02%
21	B_1	6.14	35.94	20	0.22	0.6	664	9920	611	10736	−7.98%	8.23%	600	10683	−9.64%	7.69%
22	B_1	6.13	34.24	60	0.18	0.45	685	10400	644	11009	−5.99%	5.86%	633	10764	−7.59%	3.50%
23	B_1	6.14	35.62	100	0.12	0.28	682	10100	630	10893	−7.62%	7.85%	621	10434	−8.94%	3.31%
24	B_1	6.14	35.78	160	0.11	0.2	673	10300	630	10923	−6.39%	6.05%	623	10398	−7.43%	0.95%
25	B_{10}	6.16	15.52	20	0.3	0.4	315	3670	300	3718	−4.76%	1.31%	297	3543	−5.71%	−3.46%
26	B_{10}	6.13	14.94	60	0.25	0.29	340	3890	335	3991	−1.47%	2.60%	334	3791	−1.76%	−2.54%
27	B_{10}	6.16	15.91	100	0.18	0.11	338	4060	344	4089	1.78%	0.71%	343	3846	1.48%	−5.27%
28	B_{10}	6.12	15.03	160	0.1	0.09	345	4070	354	3944	2.61%	−3.10%	354	3846	2.61%	−5.50%
29	B_{10}	6.14	34.8	20	0.3	0.7	687	10200	633	11023	−7.86%	8.07%	621	11078	−9.61%	8.61%
30	B_{10}	6.14	35.13	60	0.22	0.59	783	11700	722	12563	−7.79%	7.38%	709	12485	−9.45%	6.71%
31	B_{10}	6.14	35.78	100	0.14	0.38	721	11400	689	11968	−4.44%	4.98%	678	11607	−5.96%	1.82%
32	B_{10}	6.15	35.88	160	0.12	0.35	770	12100	731	12725	−5.06%	5.17%	720	12285	−6.49%	1.53%

where T is expressed in °C. Constants of the constitutive equation were found in [44] through regression analysis on experimental compressions test data. The flow stress model reported in Eq. 55 was used in this paper. In the resolutive algorithm of the numerical model, Eq. 55 was used at each integration point, while in the analytical model, Eq. 55 was used in order to find the mean value of flow stress $\bar{k}$. If flow stress depends only on temperature and strain rate, as in this case, the mean value of flow stress at the desired temperature can be calculated from Eq. 55 using a mean value of strain rate obtainable from Eq. 21.

5.3 Comparison of the results

Table 1 reports the comparisons between experimental measurement of rolling torque and load with both numerical and analytical models. It is important to highlight that rolling

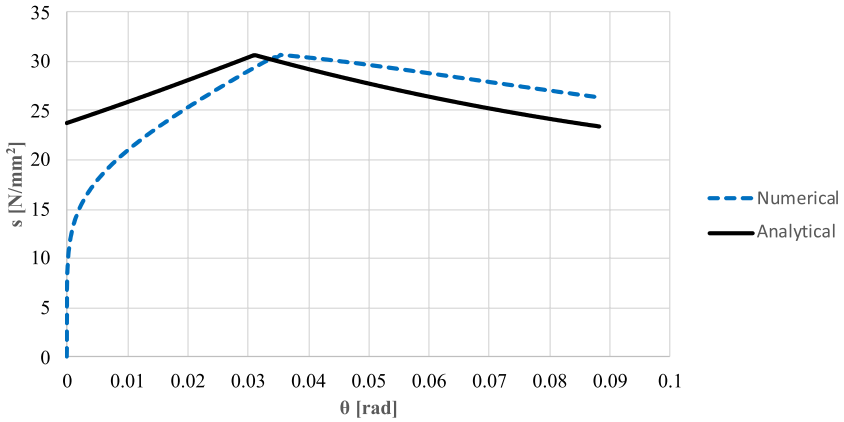

Fig. 4 Comparison between numerical and analytical solution in terms of roll's pressure distribution

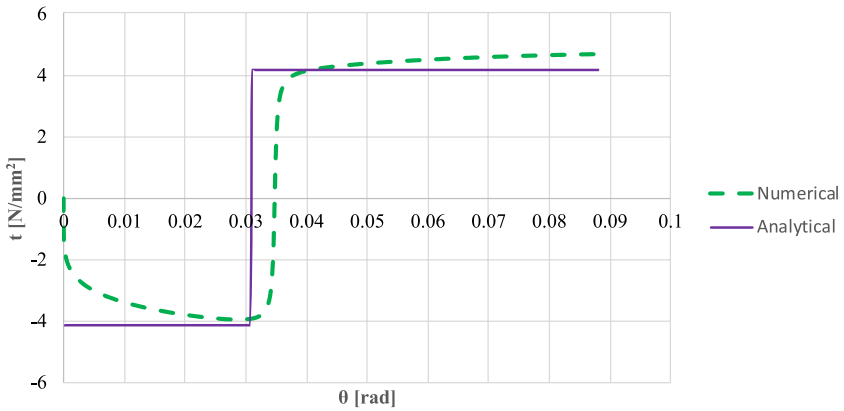

Fig. 5 Comparison between numerical and analytical solution in terms of friction stress distribution

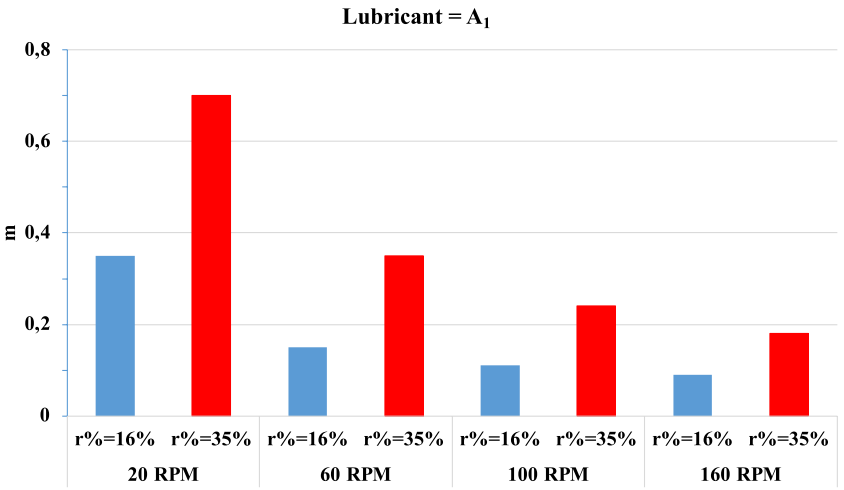

Fig. 6 - Variation of m in rolling tests performed with lubricant A_1

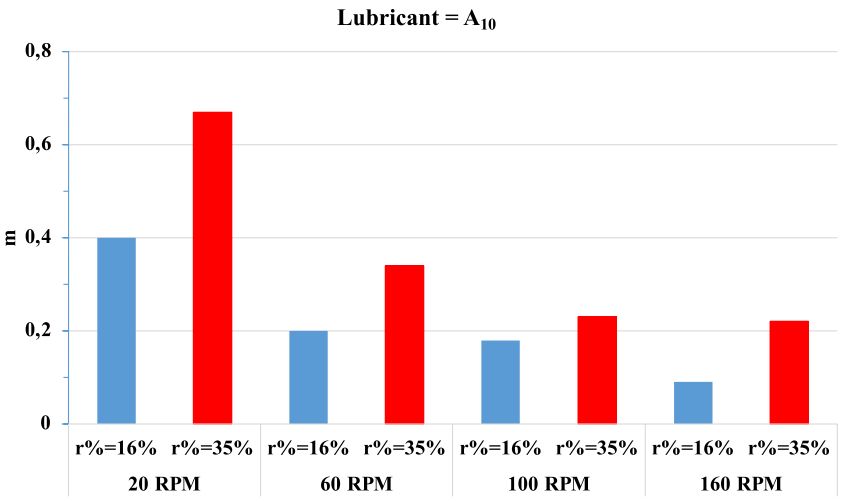

Fig. 7 - Variation of m in rolling tests performed with lubricant A_{10}

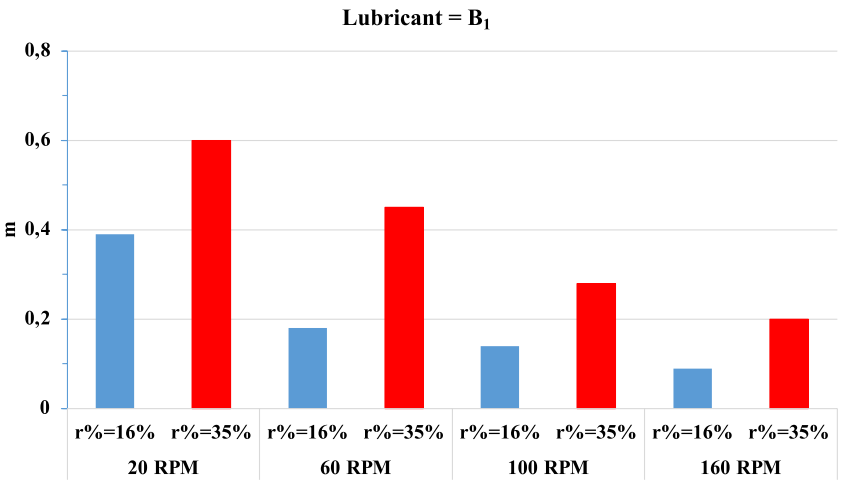

Fig. 8 - Variation of m in rolling tests performed with lubricant B_1

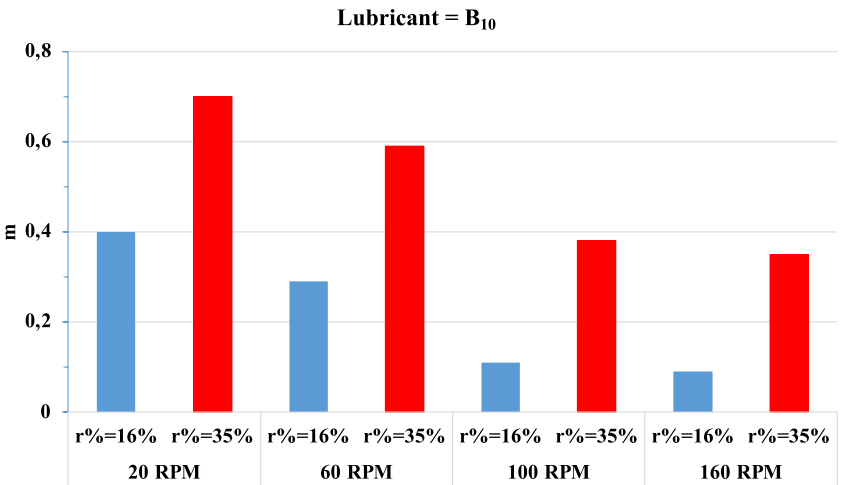

Fig. 9 - Variation of m in rolling tests performed with lubricant B_{10}

torque estimated by the proposed models refers to a single roll while experimental measurements reported in [44] refer to the total rolling torque. Therefore, for the comparison, it is necessary to double the values obtained by means of Eqs. 25 and 48.

As can be observed from Table 1, both numerical and analytical models show a good agreement with experimental measurements in terms of rolling torque and load. In particular, in the torque prediction maximum errors are less than

8.94% for the numerical model and less than 11.60% for the analytical one while in the load prediction, maximum errors are less than 9.12% and less than 10.85% respectively for the numerical and analytical model.

In Fig. 4, a comparison between numerical and analytical solution in terms of roll's pressure distribution is reported.

As it can be observed, the numerical approach is able to take into account a null value of s at the exit section ($\theta=0$) where strain rate and, as a consequence (see Eq. 47), the flow stress are equal to zero. Differently, the analytical solution, considering a mean value of the flow stress everywhere in roll bite, does not show a null value of s at the exit section ($\theta=0$). Furthermore, Fig. 5 reports a comparison between numerical and analytical solution in terms of friction stress prediction in the roll bite.

In addition to the previously mentioned differences in terms of flow stress, it is possible to observe (slope of the dotted line in Fig. 5 around the neutral point) that, thanks to Eq. 9, the numerical model is able to predict a null value of friction force at the neutral point where there is no relative velocity between rolls and workpiece speed. Analytical solution fails in this prediction and can only consider the change of friction forces direction in correspondence of the neutral point. From both Figs. 4 and 5, it can be seen that there is also a difference in the estimation of the neutral point location. This difference between numerical and analytical solution was about 10%. Table 1 reports the coefficient of Coulomb friction μ used in [44] and the friction factor m used in the models here proposed. The histograms reported in Figs. 6, 7, 8, and 9 show the values of the shear factor m as a function of rolling reduction and rolling speed for the lubricant A_1, A_{10}, B_1, and B_{10}, respectively.

The shear friction factor has been plotted against the speed of rolling in Figs. 6 and 7 for the A_1 and A_{10} — emulsion and in Figs. 8 and 9 for the B_1 and B_{10} — emulsion. From Table 1 and from the histograms of Figs. 6, 7, 8, and 9, it is possible to see that, according with Chun and Lenard [44], generally, the frictional resistance decreases if speed increases and increases as reduction increases. In effect, the shear friction factor, in rolling tests, is a critical parameter that characterizes the interface between the rolling material and the rolls during the rolling process. As the rolling reduction increases, the shear friction factor tends to increase. This is because a higher reduction in thickness leads to a greater deformation of the material, causing more interlocking and interaction between the material and the rolls. The increased contact area and deformation result in higher resistance to shear, hence an increase in the shear friction factor. Furthermore, the shear friction factor tends to decrease with an increase in rolling speed. Higher rolling speeds typically reduce the contact time between the material and the rolls, limiting the opportunity for extensive interlocking and interaction. As a result, the shear resistance decreases, leading to a lower shear friction factor. These relationships are crucial for optimizing the rolling process to achieve desired material properties and efficient manufacturing. This trend can be observed for each employed lubricant.

6 Conclusion

In this paper, a mathematical model based on slab method and able to predict rolling torque and load was proposed. Both numerical and analytical resolutions of the starting mathematical equations were developed. In this last case, useful formulas for the calculation of rolling torque and load were analytically obtained. The proposed mathematical modeling was validated by the comparison with experimental measurements concerning hot rolling of aluminum and two types of semi-synthetic lubricants found in literature. One of the oils was designed for low friction, while the other for higher friction. Both numerical and analytical calculation showed good agreement with experimental data giving a good estimation with a maximum absolute error less than 10.17% and 10.92%, respectively, for the numerical and analytical case. The obtained analytical torque formula is interesting because it can be inverted in order to obtain a quick estimation of the shear factor m once rolling torque and material flow stress are experimentally known. The estimated friction factor values used in the mathematical calculation show good agreement with the adhesion theory which states that friction forces increase as rolling speed and reduction increase.

It should be highlighted that the model studied in this paper can be used independently of the final geometry. With the appropriate modifications of the formulas, it is possible to apply the methodology to other cases with different sections (the important thing is to have a rectangular section) and different materials. Therefore, the strength of the model studied in this paper is that it can be extended to other hot plastic deformation processes.

Finally, it is good to point out that, when larger reduction ratios are involved during rolling, the constraint used in the mathematical model (conditions 1 and 2) deviates significantly more from the real-world rolling. Specifically, percentage reductions greater than 35%, translate into strong non-homogeneous deformation behaviors (sections no longer remain flat). Consequently, the model which instead assumes that the sections deform while remaining flat, overestimates the rolling loads (in fact, the non-homogeneous behavior results in a lower deformation power, consistently with the energy theorems, according to which the deformation paths occur in configurations such as to minimize the energy required). This may be a limitation of the model and, depending on the material, it is necessary to validate the applicability.

Author contribution Conceptualization, A.A.; methodology, A.A., A.D.P.; formal analysis, A.A., A.D.P., T.P.; data curation, A.A., A.D.P., T.P.; writing—original draft preparation, A.A.; review and editing, A.A., A.D.P., T.P.; supervision, A.A. All authors have read and agreed to the published version of the manuscript.

Declarations

Competing interests The authors declare no competing interests.

References

1. Barbu CD, Sandru N (2018) A rational analytical model of flat rolling problem. Acta Mech 229:3069–3088. https://doi.org/10.1007/s00707-018-2144-0
2. Wang J, Liu X, Guo W (2018) Analysis of mechanical parameters for asymmetrical strip rolling by slab method. Int J Adv Manuf Technol. https://doi.org/10.1007/s00170-018-2368
3. Montmitonnet P, Fourment L, Ripert U, Ngo QT, Alain EA (2016) State of the art in rolling process modelling. BHM Springer- Verlag Wien 161(9):396–404. https://doi.org/10.1007/s00501-016-0520-4
4. Zaaf M, Mebarek A, Amirat A (2019) Simplified two-dimensional model for the prediction of pressures and velocities in hot strip rolling. Int J Adv Manuf Technol 100:13–23. https://doi.org/10.1007/s00170-018-2691-5
5. Bogatov AA, Nukhov DS, P'yankov KP (2015) Finite element modelling of plate rolling. Metallurgist 59(1–2):113–118. https://doi.org/10.1007/s11015-015-0069-6um
6. Chandra S, Dixit US (2004) A rigid-plastic finite element analyses of temper rolling process. J Mater Process Technol 152:9–16. https://doi.org/10.1016/j.jmatprotec.2003.11.003
7. Le HR, Sutcliffe MPF (2004) Finite element modeling of the evolution of surface pits in metal forming processes. J Mater Process Technol 145:391–396. https://doi.org/10.1016/j.jmatprotec.2003.09.007
8. Boman R, Ponthot JP (2004) Finite element simulation of lubricated contact in rolling using Arbitrary Lagrangian Eulerian formulation. Comput Methods Appl Mech Eng 193(39–41):4323–4353. https://doi.org/10.1016/j.cma.2004.01.034
9. Li S, Wang Z, Ruan J, Liu C, Xu Z (2016). Hydrodynamics method and its application in hot strip rolling. Steel Res Int 87(9999). https://doi.org/10.1002/srin.201600220
10. Li S, Wang Z, Liu C, Ruan J, Xu Z (2016) A simplified method to calculate the rolling force in hot rolling. Int J Adv Manuf Technol 88:2053–2059. https://doi.org/10.1007/s00170-016-8890-z. (Springer-Verlag London)
11. Zhang DH, Yuan-Ming Liu YM, Sun J, Zhao DW (2016) A novel analytical approach to predict rolling force in hot strip finish rolling based on cosine velocity field and equal area criterion. Int J Adv Manuf Technol 84:843–850. https://doi.org/10.1007/s00170-015-7692-z
12. Rabindran R, Karhausen K, Hirt G, Teller M, Hojda S (2022) Procedure to implement shear evolution in fast rolling models with online capability on the example of an aluminum flat rolling process. Arch Appl Mech 92:3465–3502. https://doi.org/10.1007/s00419-022-02238-7
13. Lippmann H (1962) Die elementare Plastizitätstheorie der Umformtechnik. BBR8, pp 374–383
14. Lippmann H (1962) Principal line theory of axially-symmetric plastic deformation. JMPS 10:111–122. https://doi.org/10.1016/0022-5096(62)90014-5
15. Lenard JG (2014) Primeron Flat Rolling. Elsevier, Oxford
16. Montmitonnet P, Buessler P (1991) A review on theoretical analyses of rolling in Europe. Iron Steel Inst Jpn 31:525–538. https://doi.org/10.2355/isijinternational.31.525
17. Lenard JG, Pietrzyk M, Cser L (1999) Mathematical and physical simulation of the properties of hot rolled products. Elsevier, Kidlington, Oxford
18. dos Santos AA, Barbosa JV (2020) Calculation of rolling force in the hot strip finishing mill using an empirical model. Tecnol Metal Mater Miner 17(2):149–156. https://doi.org/10.4322/2176-1523.20202218. (São Paulo)
19. Montmitonnet P (2006) Hot and cold strip rolling processes. Comput Methods Appl Mech Eng 195(48–49):6604–6625
20. Von Karman T (1925) Beitrag zur Theorie des Walzvorganges. ZAMM 5(1):139–141
21. Bland DR, Ford H (1948) The calculation of roll force and torque in cold strip rolling with tensions. Proc Inst Mech Eng 159(1):144–163
22. Zhang D-W, Fang-Fang Xu, Zai-Chi Yu, Kun-Yin Lu, Zheng Z-B, Zhao S-D (2021) Coulomb, Tresca and Coulomb-Tresca friction models used in analytical analysis for rolling process of external spline. J Mater Process Tech 292:117059. https://doi.org/10.1016/j.jmatprotec.2021.117059
23. Bland DR, Ford H (1952) Cold rolling with strip tension-Part III: an approximate treatment of the elastic compression of the strip in cold rolling. J Iron Steel Inst 171:245–249
24. Orowan E (1943) The calculation of roll pressure in hot and cold flat rolling. Proc Inst Mech Engrs 150(1):140–167
25. Sims RB (1954) Calculation of roll force and torque in cold rolling by graphical and experimental methods. J Iron Steel Inst 178:19–34
26. Sims RB (1954) Calculation of roll force and torque in hot rolling mills. Proc Inst Mech Eng 168(1):191–200
27. Alexander JM (1972) On the theory of rolling. Proc R Soc London A 326(1):535–563
28. Pietrzyk M, Lenard JG (1991) Thermal-mechanical modelling of the flat rolling process. Springer-Verlag, Berlin
29. Gunasekera JS, Alexander JM (1987) Analysis of rolling. Ann CIRP 36(1):203–206
30. Rusia D (1990) Improvements to Alexander's computer model for force and torque calculations in strip rolling processes. J Mater Shap Technol 8(3):167–177
31. Chen CC, Kobayashi S (1978) Rigid-plastic finite element analysis of ring compression. Application of numerical methods to forming processes
32. Venter R, Abd-Rabbo A (1980) Modelling of the rolling process—I: inhomogeneous deformation model. Int J Mech Sci 22(2):83–92
33. Venter RD, Abd-Rabbo A (1980) Modelling of the rolling process—II: evaluation of the stress distribution in the rolled material. Int J Mech Sci 22(2):93–98
34. Freshwater IJ (1996) Simplified theories of flat rolling—I: the calculation of roll pressure, roll force and roll torque. Int J Mech Sci 38(6):633–648
35. Lalli LA (1984) An analytical rolling model including through thickness shear stress distribution. ASME J Eng Mater Technol 106(1):1–8
36 Hu P, Ehmann KF (2000) A dynamic model of the rolling process. Part I: homogeneous model. Int J Mach Tools Manuf 40(1):1–19
37. Yang Y, Peng Y (2021) Theoretical model and experimental study of dynamic hot rolling. Metals 11(9):1346. https://doi.org/10.3390/met11091346
38. dos Santos AA, Barbosa JV (2020) Calculation of rolling force in the hot strip finishing mill using an empirical model. Tecnol Metal Mater Miner 17(2):149–156 (São Paulo)
39. Schultz RG, Smith AW Jr (1965) Determination of a mathematical model for rolling mill control. Iron Steel Eng 80:127–133

40. Baranov G (2020) Improvement of Methods of Calculation of forces in hot strip rolling. https://doi.org/10.4028/www.scientific.net/SSP.299.577
41. Li Si, Wang Z, Guo Y (2019) A novel analytical model for prediction of rolling force in hot strip rolling based on tangent velocity field and MY criterion. J Manuf Process 47:202–210
42. Li L, Xie H, LiuT, HuoM, Liu X, Li X, Shi K, Li J, Liu H, Sun L, Jiang Z (2022) Influence mechanism of rolling force on strip shape during tandem hot rolling using a novel 3D multi-stand coupled thermo-mechanical FE model. https://doi.org/10.1016/j.jmapro.2022.07.025
43 Hu P, Ehmann KF (2000) A dynamic model of the rolling process. Part II: inhomogeneous model. Int J Mach Tools and Manuf 40(1):21–31
44. Chun MS, Lenard JG (1997) Hot rolling of an aluminum alloy using oil/water emulsions. J Mat Proc Tech 72(2):283–292
45. Liu T, Jiang H, Sun H, Wang Y, Dong Q, Zeng J, Bian F, Zhang J, Chen F, Sun B (2022) Effects of rolling deformation on precipitation behavior and mechanical properties of Al–Zn–Mg–Cu alloy. Mater Sci Eng A 847:143342
46. Jiang HJ, Liu CY, Chen Y, Yang ZX, Huang HF, Wei LL, Li YB, Qi HQ (2018) Evaluation of microstructure, damping capacity and mechanical properties of Al-35Zn and Al-35Zn-05.Sc alloys. J Alloys Compd 739:114e121
47. Rajak MK, Mondal DP, Mehta Y (2023) Effect of rolling on microstructure behaviour, and mechanical properties of Mg-Al-Si alloys. Mater Today Commun 35:106320
48. Gao Z, Kang Q, An X, Wang H, Wang C, Cao W (2023) Enhanced mechanical properties of a Fe-Mn-Al-C austenitic low-density steel by increasing hot-rolling reduction. Mater Charact 204:113237
49. Kraner J, Cvahte P, Šuštaricˇ P, Šuštar T, Donik C, Paulin I, Kim SK, Il Kim K (2023) Effects of variated final temperature and workpiece thickness for hot rolling of aluminum alloy EN AW-8011. Metals 13:1301. https://doi.org/10.3390/met13071301
50. Chen J, Liu C, Guana R, Wen F, Zhou Q, Zhao H (2020) Improving the comprehensive mechanical property of the rheo-extruded Al-Fe alloy by severe rolling deformation. J Mater Res Technol 9(2):1768–1779
51. Lee J-H, Park L-J, Kim S-B, Paik K-W (1999) The effect of reduction ratio of hot rolling on texture and secondary recrystallization of MA 754 plate. J Mater Sci Lett
52. Lv Y-Y, Zhang L-F, Wang G-X, Xiong Y (n.d.) Effect of rolling and annealing on microstructure and mechanical properties of high purity aluminum. Adv Eng Res 110
53. Timoshenko S (1940) Strength of materials, elementary theory and problems
54. Timoshenko S (n.d.) Theory of elasticity, October 1970
55. Timoshenko S (n.d.) Theory of plates and shells, July 1989.
56. Ngo QT (2015) Thermo-elasto-plastic uncoupling model of width variation for online application in automotive cold rolling process. PhD thesis 2015. École doctorale Sciences, Ingénierie et Environnement (Champs-sur-Marne, Seine-et-Marne ; 2010–2015)
57. Quarteroni A, Saleri F, Gervasio P (2002) Calcolo Scientifico. Springer-Verlag Italia Srl
58. Wang J, Liu X, Sun X (2020) Study on asymmetrical cold rolling considered sticking friction. J Mater Res Technol 9(6):14131–14141
59. Pasoodeh B, Tagimalek H (2020) Analytical and numerical evaluation of wire flat rolling process based on the slab method and DEFORM-3D. J Adva Mater Process 8(4):3–16 (Autumn)